Environmental Science: Atmospheres

ROYAL SOCIETY OF CHEMISTRY

PAPER

View Article Online
View Journal

Cite this: DOI: 10.1039/d5ea00069f

Impact of particle phase state on the competition between condensation and coagulation

Kieudiem Nguyen, Meredith Schervish, Pascale S. J. Lakey, James N. Smith and Manabu Shiraiwa *

The evolution of particle size distribution of secondary organic aerosols (SOAs) is influenced by condensation and coagulation. Amorphous semisolid and glassy states in SOAs cause kinetic limitations for condensational growth, but the impact of these phase states on the competition between condensation and coagulation has not been evaluated. In this work, we implement coagulation into the kinetic multilayer model of gas–particle interactions (KM-GAP) to calculate the timescales of SOA partitioning and coagulation for liquid, semisolid, and highly viscous particles for closed and open systems. We find that the phase state may not have a major impact on the coagulation timescale, with particle size playing a more critical role. The equilibration timescale of SOA partitioning is shorter than the coagulation timescale for most conditions in the closed system, while coagulation becomes competitive especially for high particle number concentration and the highly viscous phase state ($D_b \leq 10^{-15}$ cm^2 s^{-1}) due to the prolonged timescale of partitioning. We also illustrate that coagulation is less significant for the growth of seed particles in chamber experiments even for viscous particles, as the condensation sink of low volatility compounds would be larger than the coagulation sink due to their efficient mass accommodation. Coagulation becomes important during nanoparticle growth and the interplay between condensation and coagulation can result in the emergence of a bimodal size distribution with nanoparticles likely adopting a low viscosity phase state. Coagulation is also important for size distribution dynamics in a smoke plume for highly viscous submicron particles as their evaporation and condensation are inhibited with kinetic limitations.

Received 18th June 2025
Accepted 14th November 2025

DOI: 10.1039/d5ea00069f

rsc.li/esatmospheres

Environmental significance

The competition of condensation and coagulation is important in determining the evolution of particle size distribution and potential of nanoparticles to grow to cloud condensation nuclei. For particles with low viscosity, condensation tends to dominate and grow particles efficiently. Coagulation becomes a competitive process for highly viscous particles, modulating particle size distribution dynamics especially during new particle formation and biomass burning plumes with high particle number concentrations.

Introduction

Secondary organic aerosols (SOAs) are ubiquitous in the atmosphere, accounting for a large fraction of submicron particles.[1] They impact climate, air quality, and public health.[2–4] SOAs are generated through oxidation of volatile organic compounds (VOCs) emitted from anthropogenic and biogenic sources to form semi-volatile and low-volatile organic compounds, which can subsequently condense into preexisting particles.[5,6] The size of an SOA particle affects how it scatters and absorbs incoming solar radiation, as well as its ability to form clouds, influencing the Earth's radiation and climate.[7] When the nanoparticles grow to ~100 nm in diameter, they can potentially serve as cloud condensation nuclei (CCN).[8] The growth and survival of nanoparticles to CCN-relevant sizes are governed by the competing dynamic processes of condensation growth and coagulation loss.[9] The condensation process involves a series of mass transport processes including gas-phase diffusion, gas-surface transfer, surface–bulk exchange, and bulk diffusion within the particle.[10] These processes are often represented as fast relative to the timescales of other atmospheric processes, as SOA particles were traditionally assumed to be homogeneous and quasi-liquid droplets.[11]

Laboratory experiments and atmospheric measurements have demonstrated SOA particles can adopt liquid (dynamic viscosity $\eta \leq 10^2$ Pa s), semi-solid ($10^2 \leq \eta \leq 10^{12}$ Pa s), or glassy ($\eta \geq 10^{12}$ Pa s) states, depending on chemical composition, relative humidity, and temperature.[12–14] Global and regional modeling studies suggested that SOA particles exist in an

Department of Chemistry, University of California, Irvine, USA. E-mail: m.shiraiwa@uci.edu

amorphous solid or glassy state in the free troposphere and over deserts with low relative hudmidity.[15–20] This can lead to prolonged characteristic bulk diffusion timescales of organic molecules within SOA particles[21,22] and facilitate long-range transport of toxic organic compounds in the atmosphere.[23,24] Modeling studies also demonstrated that partitioning of semi-volatile compounds into highly viscous aerosols leads to kinetically-limited growth with prolonged equilibration timescales of SOA partitioning[25] and particle–particle mixing timescales,[26,27] thus affecting the evolution of particle size distributions upon SOA growth.[28–33]

Coagulation is a kinetic process in which two particles collide and stick together to form a larger particle. Coagulation reduces the number of particles while conserving the particle volume concentration.[9] Chamber and flow tube experiments often reduce the impact of coagulation by keeping the particle concentration low or residence times short;[28,34–36] however, particle concentrations cannot be controlled in new particle formation chamber experiments, so it is important to account for coagulation. This drives the need to better understand how the particle phase state impacts the interplay of condensation and coagulation, which determines the evolution of particle size distributions.

In this study, we apply the kinetic multilayer model of gas–particle interactions in aerosols and clouds (KM-GAP)[28,37] to investigate the timescales of condensation and coagulation of aerosols under the combined impacts of particle phase state and volatility of condensing species. We simulate the evolution of particle size distribution to illustrate the competition of condensation and coagulation in laboratory chamber experiments of growth of SOA and freshly nucleated particles as well as the evolution of particle size distribution in a biomass burning plume. The modeling results are compared with experimental and modeling studies for each scenario to provide a better understanding of the competition between condensation and coagulation.

Method

KM-GAP is used to simulate the evolution of particle size distribution by condensation and coagulation. KM-GAP consists of multiple model compartments and layers: a gas phase, a near-surface gas phase, a sorption layer, a near surface bulk layer, and ten bulk layers.[28,37] The processes that are explicitly considered in KM-GAP are gas-phase diffusion, adsorption and desorption, surface–bulk exchange, and bulk diffusion. For size-resolved simulations, the bin method with a fully mobile size structure is used, in which the particle sizes change in each size bin due to condensation.

Coagulation has previously not been treated in KM-GAP. In this study, we implemented coagulation in KM-GAP by including eqn (1), which describes the change in number concentration in particle size bin k (N_k, in cm^{-3}) due to coagulation:[38,39]

$$\frac{\mathrm{d}N_k(t)}{\mathrm{d}t} = \frac{1}{2}\sum_{j=1}^{k}\left(\sum_{i=1}^{k}\frac{v_i+v_j}{v_k}f_{i,j,k}K_{i,j}N_iN_j\right) - N_k\sum_{j=1}^{N_{\mathrm{bin}}}K_{k,j}N_j \quad (1)$$

where N_i and N_j are the number concentration of particles and v_i and v_j are the single particle volume in the size bin i and j (cm^{-3}), respectively. $K_{i,j}$ is the Brownian coagulation coefficient (cm^3 s^{-1}) for collision between particles in the size bin i and j (see Table S1 for calculation). N_{bin} is the number of size bins. The first term in eqn (1) represents an increase of particle number concentration in the size bin k by coagulation of smaller particles and the second term accounts for coagulation loss of particles in the size bin k. To conserve mass concentration of particles upon coagulation, we apply $f_{i,j,k}$, which is the volume fraction of a coagulated pair i,j partitioned into bin k as calculated from:[40]

$$f_{i,j,k} = \begin{cases} \left(\dfrac{v_{k+1}-V_{i,j}}{v_{k+1}-v_k}\right)\dfrac{v_k}{V_{i,j}}, & v_k \le V_{i,j} < v_{k+1};\ \ k < N_{\mathrm{bin}} \\ 1 - f_{i,j,k-1}, & v_{k-1} < V_{i,j} < v_k\ ;\ \ k > 1 \\ 1, & V_{i,j} \ge v_k;\ \ k = N_{\mathrm{bin}} \\ 0, & \text{all other cases} \end{cases} \quad (2)$$

where $V_{i,j} = v_i + v_j$ is the total volume of the coagulated particle from size i and j, having volume v_i and v_j, respectively. This coagulated particle, which falls between the volumes of two model size bins, k and $k+1$ with volume v_k and v_{k+1}, respectively, is partitioned in these two bins. We assumed that particles have the same chemical composition in each size bin, and they do not grow out of the largest size bin in the distribution after coagulation.

The model simulations are mainly conducted with a closed system, in which condensation of species would lead to a decrease in its gas phase mass concentration and an increase in its particle phase mass concentration. The closed system represents chamber experiments in batch mode. Additional simulations with an open system with a fixed gas phase concentration were also conducted to represent chamber experiments under continuous flow and ambient conditions where the condensing species may be continuously generated. The surface accommodation coefficient is set to 1 based on molecular dynamics simulations.[41,42] We simulate different phase states of particles with typical bulk diffusivities $D_{\mathrm{b}} = 10^{-8}$ cm^2 s^{-1} for a liquid particle, $D_{\mathrm{b}} = 10^{-15}$ cm^2 s^{-1} for a semisolid particle, and $D_{\mathrm{b}} = 10^{-17}$ cm^2 s^{-1} for a highly viscous particle. These diffusivities are chosen to represent a range found in atmospherically relevant aerosol particles.[21] D_{b} is fixed at any given depth in the particle bulk for each simulation, assuming condensation of semi-volatile compounds would not alter particle viscosity and diffusivity. We did not consider potential viscosity/diffusivity change, which is beyond the scope of this manuscript. The volatility, expressed as the pure compound saturation mass concentration (C^0) of condensing species, and the particle number concentration are also varied.

To examine how the competition between condensation and coagulation is affected by the particle phase state, we evaluate the equilibration timescale of SOA partitioning (τ_{eq}) and characteristic coagulation timescale (τ_{coag}) by simulating condensation of species Z into pre-existing non-volatile polydispersed particles. τ_{eq} is calculated as the e-folding time when the

condensing species (Z) achieves equilibrium in the particle phase, which is the first time (t) at which the following condition is satisfied:[43]

$$\frac{|C_p(t) - C_{p,eq}|}{|C_{p,0} - C_{p,eq}|} < \frac{1}{e} \quad (3)$$

where $C_{p,0}$ and $C_{p,eq}$ are the mass concentration of Z in the particle phase at the initial condition and at equilibrium, respectively.

Following common practice, τ_{coag} is defined as the time needed for reduction of the initial particle number concentration to half its initial value.[38] For monodispersed and polydispersed particles, τ_{coag} can be calculated numerically from the decrease of the total particle number concentration in KM-GAP simulations. Additionally, for monodispersed particles with particle diameter D_p, the self-coagulation timescale (τ_{scoa}) can be calculated analytically as follows:[38,44]

$$\tau_{scoa} = \frac{2}{KN_0} \quad (4)$$

where N_0 is initial particle number concentration and K is the coagulation coefficient. K is a function of particle diameter, Brownian diffusivity of a particle, mean thermal velocity of a particle, and coagulation efficiency (see Table S1 for equations). For derivation of eqn (4), the coagulation coefficient is assumed to be constant for monodispersed particles. K is a function of coagulation efficiency (α), which represents the fraction of collisions that result in coagulation. Coagulation efficiency is size-dependent: it decreases as the particles get smaller and can decrease down to 0.1 for nanoparticles.[45,46] Previous modeling studies have shown that coagulation efficiency of soot particles is much lower compared to that of similarly sized metal nanoparticles due to shallower attractive forces upon collision.[47] This suggests that glassy viscous particles might exhibit a lower coagulation efficiency. Therefore, we calculated τ_{scoa} for monodispersed particles with coagulation efficiency of 1 and 0.1 to explore its influence on τ_{scoa}.

Fig. 1 shows τ_{scoa} for monodispersed particles as a function of particle diameter (D_p = 1 nm–10 μm) and particle number concentrations ($N_0 = 10^3$–10^8 cm^{-3}) with α of 1 and 0.1. For both cases, higher N_0 leads to shorter τ_{scoa} as it increases the probability of two particles to collide and coagulate. For a given N_0, coagulation is more efficient with shorter τ_{scoa} for D_p in the 10–100 nm size range due to their relatively high mobility leading to higher coagulation coefficient. When the coagulation efficiency is decreased to 0.1, τ_{scoa} of particles in the 1–10 nm size range increase an order of magnitude due to their small cross-sectional area, which reduces the probability of coagulation. τ_{scoa} of larger particles is slightly increased, but within an order of magnitude compared to τ_{scoa} with α of 1. This suggests that τ_{scoa} of larger particles is less sensitive to the changing collision efficiency. Nanoparticles (D_p < 20 nm) were observed to bounce less on an impactor[12,48] and they tend to adopt a less viscous phase state due to the nanosized effect, which suppresses the glass transition temperature.[49,50] Thus, the phase state may not have a major impact on the coagulation timescale, with particle size playing a more dominant role.

In order to compare condensation and coagulation scavenging rates for a specific size of particles, we calculate the timescales of coagulation ($\tau_{coag,i}$) and condensation ($\tau_{cond,i}$). The removal timescale of particles in the size bin i due to coagulation with other particles is the inverse of the coagulation sink for a specific size which determines the amount of time for the particles in size bin i to be removed through coagulation:[51]

$$\tau_{coag,i} = \frac{1}{CoagSink_i} = \frac{1}{\sum_{j=1}^{N_{bin}} K_{i,j} N_j} \quad (5)$$

where $K_{i,j}$ is the coagulation coefficient between particle size i and j. N_j is the particle number concentration in the size bin j.

The condensation timescale (τ_{cond}) is the inverse of the condensation sink, which determines the loss of vapors onto surfaces of the existing particles:[44,51]

$$\tau_{cond,i} = \frac{1}{CS_i} = \frac{1}{2\pi D_g D_{p,i} \beta(Kn_i, \alpha_{eff,i}) N_i} \quad (6)$$

where D_g is the gas-phase diffusion (cm^2 s^{-1}), and $D_{p,i}$ and N_i are the particle diameter and number concentration in the size bin i. $\beta(Kn_i,\alpha_{eff,i})$ is the transition regime correction factor which is dependent on particle Knudsen number (Kn) and effective mass

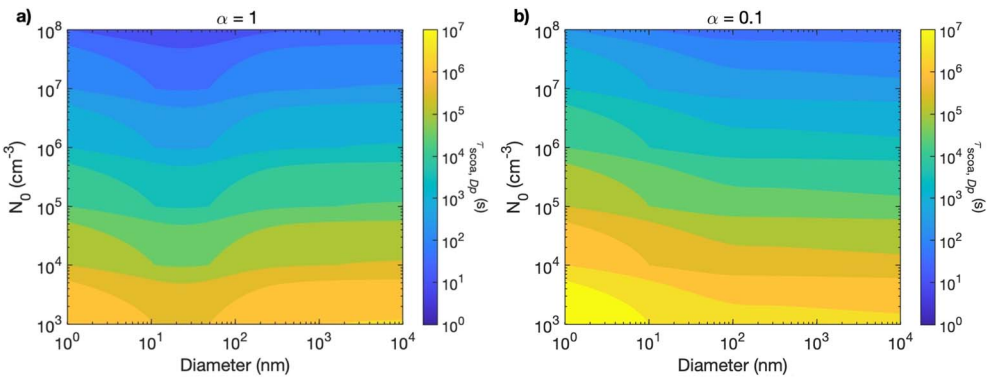

Fig. 1 Characteristic self-coagulation timescale (τ_{scoa}) for monodispersed particles as a function of particle diameter (D_p = 1 nm–10 μm) and particle number concentrations ($N_0 = 10^3$–10^8 cm^{-3}) with different coagulation efficiencies: (a) α = 1, (b) α = 0.1.

accommodation coefficient ($\alpha_{\mathrm{eff},i}$). $\alpha_{\mathrm{eff},i}$ is the probability of a gas molecule colliding with the surface to effectively enter the particle bulk, which can be calculated by accounting for kinetic limitations of bulk diffusion:[52]

$$\alpha_{\mathrm{eff},i} = \alpha_{\mathrm{s}} \frac{1}{1 + \left(\frac{\alpha_{\mathrm{s}}\omega C^0}{4D_{\mathrm{b}}\rho_{\mathrm{p}}}\right)\frac{r_{\mathrm{p},i}}{5} \times 10^{-12}} \quad (7)$$

where α_{s} is the surface accommodation coefficient assumed to be 1, ω is the mean thermal velocity (cm s^{-1}), C^0 is the pure compound saturation mass concentration of condensing species (μg m^{-3}), D_{b} is the particle bulk diffusivity ($\mathrm{cm}^2\ \mathrm{s}^{-1}$), ρ_{p} is the particle density (g cm^{-3}), and $r_{\mathrm{p},i}$ is the radius of particle size i (cm). $\alpha_{\mathrm{eff},i}$ provides an efficient way of accounting for bulk diffusivity so that τ_{cond} considers the effect of the particle phase state and size on SOA partitioning. Note that τ_{cond} is different from τ_{eq}, which represents the e-folding time for condensing species to achieve equilibrium with the total particle population. τ_{cond} represents the timescale of growth of particles with a specific size *via* condensation.

Results and discussion

We conducted KM-GAP simulations to investigate the competition of condensation and coagulation (τ_{eq} *vs.* τ_{coag}) on particle number concentrations and the volatility of the condensing species in the closed and open systems. Then we applied KM-GAP to explore the influence of the particle phase state on the competition between condensation and coagulation by simulating the growth of particles in chamber experiments and in biomass burning plumes. It is important to note that the aim of this study is not to reproduce the experimental results, but rather to simulate exemplary conditions to probe the interplay and competition of condensation and coagulation.

Equilibration timescales of SOA partitioning (τ_{eq}) *vs.* coagulation timescales (τ_{coag})

In this section, the competition between condensation and coagulation is investigated for a system consisting of pre-existing seed particles and a condensing vapor. Specifically, the model simulates the condensation of semi-volatile species with pure compound saturation mass concentration of $C^0 = 10^{-1}$–10^3 μg m^{-3} into pre-existing non-volatile particles with an initially lognormal size distribution with the mean diameter of 100 nm and geometric standard deviation of 0.3. The particle phase state is assumed to be liquid with $D_{\mathrm{b}} = 10^{-8}$ $\mathrm{cm}^2\ \mathrm{s}^{-1}$, semi-solid with $D_{\mathrm{b}} = 10^{-15}$ $\mathrm{cm}^2\ \mathrm{s}^{-1}$ and highly viscous with $D_{\mathrm{b}} = 10^{-17}$ $\mathrm{cm}^2\ \mathrm{s}^{-1}$. We assume instantaneous coalescence with coagulation efficiency of 1 for all cases. The initial gas-phase mass concentration of condensing species is set at 10^{-2} μg m^{-3}. The condensing species is assumed to have a molar mass of 200 g mol^{-1} and density of 1.4 g cm^{-3}, which are assumed to be the same for non-volatile species. The particle number concentration varies from 10^3 to 10^8 cm^{-3} which covers particle concentrations from suburban clean environments to heavily polluted areas in megacities.[53,54] The simulations are conducted for both closed and open systems at 298 K and 1 atm. The parameters are summarized in Table S2.

Fig. 2 shows the simulated τ_{eq} (solid lines) and τ_{coag} (black dashed lines) as a function of particle number concentration (N_{p}). τ_{coag} decreases from ~10^6 s at $N_{\mathrm{p}} = 10^3$ cm^{-3} to ~10 s at $N_{\mathrm{p}} = 10^8$ cm^{-3} and it is independent of the volatilities of condensing species. τ_{eq} varies from seconds to months depending on particle concentrations, the volatility of the condensing species, and the particle phase state.[43,55] When the particle is liquid ($D_{\mathrm{b}} = 10^{-8}$ $\mathrm{cm}^2\ \mathrm{s}^{-1}$) in the closed system (Fig. 2a), τ_{eq} is <~100 s, depending mainly on N_{p}. Higher N_{p} means higher surface concentration, resulting in a higher condensation sink and a shorter τ_{eq}. When $N_{\mathrm{p}} > 10^6$ cm^{-3}, condensation is limited by gas diffusion and accommodation; hence, τ_{eq} does not depend on the volatility of the condensing species. When $N_{\mathrm{p}} < 10^6$ cm^{-3}, τ_{eq} is influenced by the volatility of the condensing species: τ_{eq} is shorter with higher C^0 as only small amounts need to partition to reach equilibrium, while τ_{eq} is longer with lower C^0 as more mass needs to be transported from the gas to particle phase. Overall, condensation is a dominant process over coagulation as τ_{eq} is always shorter than τ_{coag} for liquid particles in the closed system.

When the particle is semi-solid with $D_{\mathrm{b}} = 10^{-15}$ $\mathrm{cm}^2\ \mathrm{s}^{-1}$, τ_{eq} is longer compared to liquid particles due to the kinetic limitations of bulk diffusion, but still shorter than τ_{coag} (Fig. 2b). The opposite trend in volatility is found for τ_{eq}, which is shorter for lower volatility compounds. This is consistent with previous work on the effect of volatility on the equilibration timescales in a closed system.[25,43] For compounds with higher C^0, re-evaporation from semi-solid particles is significant due to slow surface–bulk exchange and bulk diffusion, leading to an increase in τ_{eq}. τ_{eq} is shorter for compounds with lower C^0 in the absence of re-evaporation due to their low volatility nature, leading to a faster establishment of local thermodynamic equilibrium between the gas-phase and near-surface bulk.[6,56] As shown in Fig. 2c, τ_{eq} becomes an order of magnitude longer when the particle is highly viscous with $D_{\mathrm{b}} = 10^{-17}$ $\mathrm{cm}^2\ \mathrm{s}^{-1}$ compared to the semi-solid. For semi-volatile compounds with $C^0 \geq 10^2$ μg m^{-3}, τ_{eq} is longer than τ_{coag}, indicating that coagulation is a competitive process with condensation. Nevertheless, condensation is a dominant process over coagulation for most conditions in the closed system.

In the open system, τ_{eq} becomes significantly longer as more mass must be transported from the gas to particle phase, as also demonstrated by previous modeling studies.[25,43,57] τ_{eq} is longer with higher N_{p} with higher absorbing mass. For liquid particles with $D_{\mathrm{b}} = 10^{-8}$ $\mathrm{cm}^2\ \mathrm{s}^{-1}$, τ_{eq} for semi-volatile compounds is still shorter than τ_{coag} (Fig. 2d). τ_{eq} of low-volatile compounds becomes longer than τ_{coag} especially at high N_{p}. τ_{eq} for semi-solid (Fig. 2e) and highly viscous particles (Fig. 2f) is less sensitive to C^0 because the timescale to achieve equilibrium is primarily controlled by bulk diffusion. In these cases, coagulation plays an increasingly significant role when the timescale for achieving equilibrium is extended due to bulk diffusion limitations. While condensation of low-volatile organic

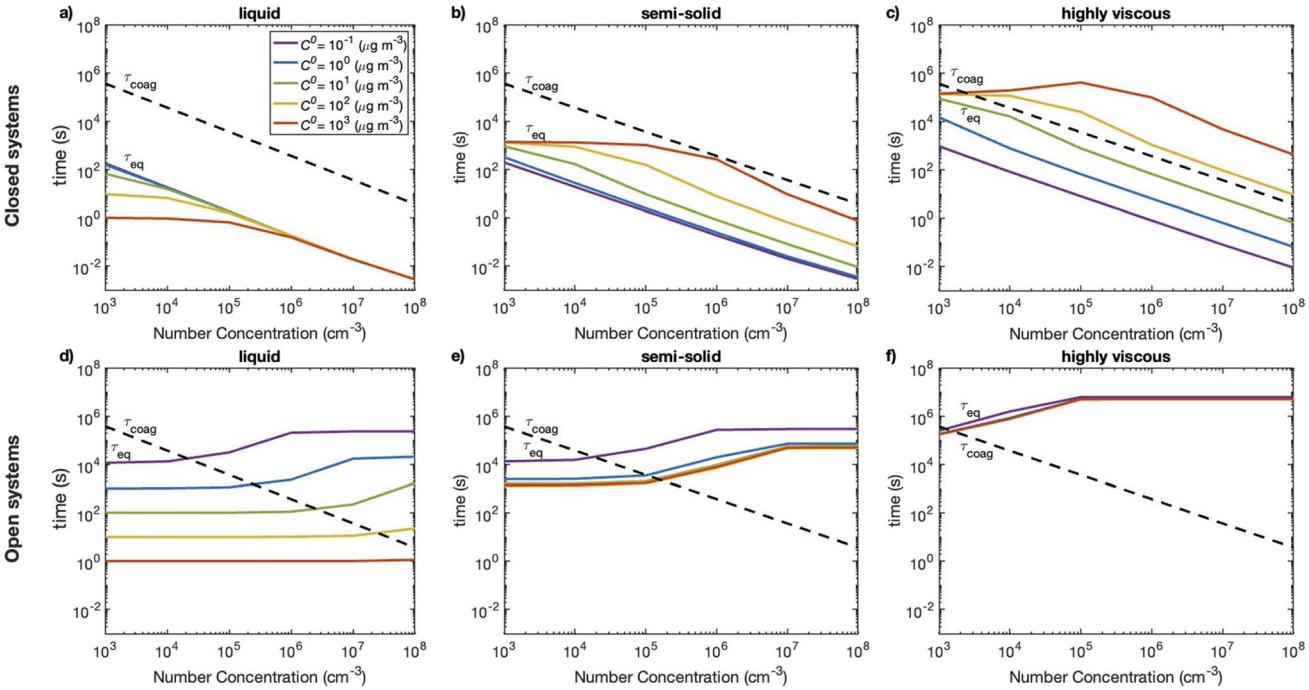

Fig. 2 Equilibration timescales of SOA partitioning (τ_{eq}, solid lines) and coagulation timescales (τ_{coag}, black dashed line) as a function of particle number concentration (10^3–10^8 cm^{-3}) for (a and d) liquid with bulk diffusivity $D_b = 10^{-8}$ cm^2 s^{-1}, (b and e) semisolid with $D_b = 10^{-15}$ cm^2 s^{-1}, and (c and f) highly viscous particles with $D_b = 10^{-17}$ cm^2 s^{-1}. The top panels represent the closed system, while the bottom panels are for the open system. τ_{eq} was calculated for species with different volatilities ($C^0 = 10^{-1}$–10^3 μg m^{-3}).

compounds (LVOCs) continues to occur, the prolonged equilibration allows coagulation to become competitive, especially for the highly viscous phase state and high particle number concentration.

Growth of SOAs in chamber experiments

We simulated the growth of SOAs from oxidation products of α-pinene ozonolysis in the presence of seed particles, which have been widely studied in chamber experiments.[58,59] The initial size distribution of non-volatile seed particles was assumed with a mean diameter of 100 nm and particle number concentrations of 4×10^3 cm^{-3} and 2×10^4 cm^{-3}, which correspond to seed mass concentrations of 5 μg m^{-3} and 20 μg m^{-3}, respectively.[59] The initial gas-phase concentration of α-pinene ($C^0 = 10^7$ μg m^{-3}) was set to be 50 μg m^{-3}, corresponding to 9 ppb at 1 atm and 298 K. For simplicity, we consider two products with semi-volatile (SVOC; $C^0 = 1$ μg m^{-3}) and low-volatile organic compounds (LVOC; $C^0 = 10^{-2}$ μg m^{-3}). The gas-phase yields from α-pinene ozonolysis for SVOC and LVOC were assumed as 0.3 and 0.14, respectively, based on a previous study.[60] The second-order rate constant of α-pinene and ozone is set to be 8×10^{-17} cm^3 s^{-1}.[61] Particle-phase reactions are not considered as we aim to focus on the particle growth primarily driven by condensable vapor and coagulation. The effect of the phase state is considered with different bulk diffusivities ($D_b = 10^{-8}$, 10^{-15}, 10^{-18} cm^2 s^{-1}). Losses of particles and vapors on walls are not treated for simplicity.

Fig. 3 shows the evolution of particle number size distribution for semi-solid particles ($D_b = 10^{-15}$ cm^2 s^{-1}) with initial seed mass concentrations of (a, c) 5 μg m^{-3} ($N_p = 4 \times 10^3$ cm^{-3}) and (b, d) 20 μg m^{-3} ($N_p = 2 \times 10^4$ cm^{-3}), showing that the particle mean diameter increases from 100 nm to ~240 nm and ~170 nm, respectively, in 12 hours. For seed mass concentrations of 5 μg m^{-3}, the modeled size distribution narrows in the first few hours, which is characteristic of gas-phase diffusion limited condensational growth.[62] As the condensable vapor concentration decreases, the size distribution shifts slightly toward larger sizes with slow condensation after 6 h. This continuous growth in particle size suggests that condensation is a dominant process over coagulation. In contrast, at a higher seed concentration of 20 μg m^{-3}, the modeled number size distribution initially narrows in the first hour but subsequently broadens, which is associated with reduction of particle number concentration after 6 h. This indicates that coagulation becomes important prominently impacting the size distribution due to high particle concentrations favoring coagulation. A similar behavior is observed in the case of liquid particles ($D_b = 10^{-8}$ cm^2 s^{-1}), as shown in Fig. S1.

To investigate the effect of seed particle diameters, we conducted simulations with an initial seed mean diameter of 200 nm with number concentrations of 5×10^3 cm^{-3} corresponding to 50 μg m^{-3}.[63] The model simulation in Fig. S2 shows that SOA particles grow to ~300 nm in 6 h with a narrowing of the characteristic size distribution, indicating the dominance of condensation. Afterwards, particles grow only slightly with a broadening of the size distribution and a slight reduction of

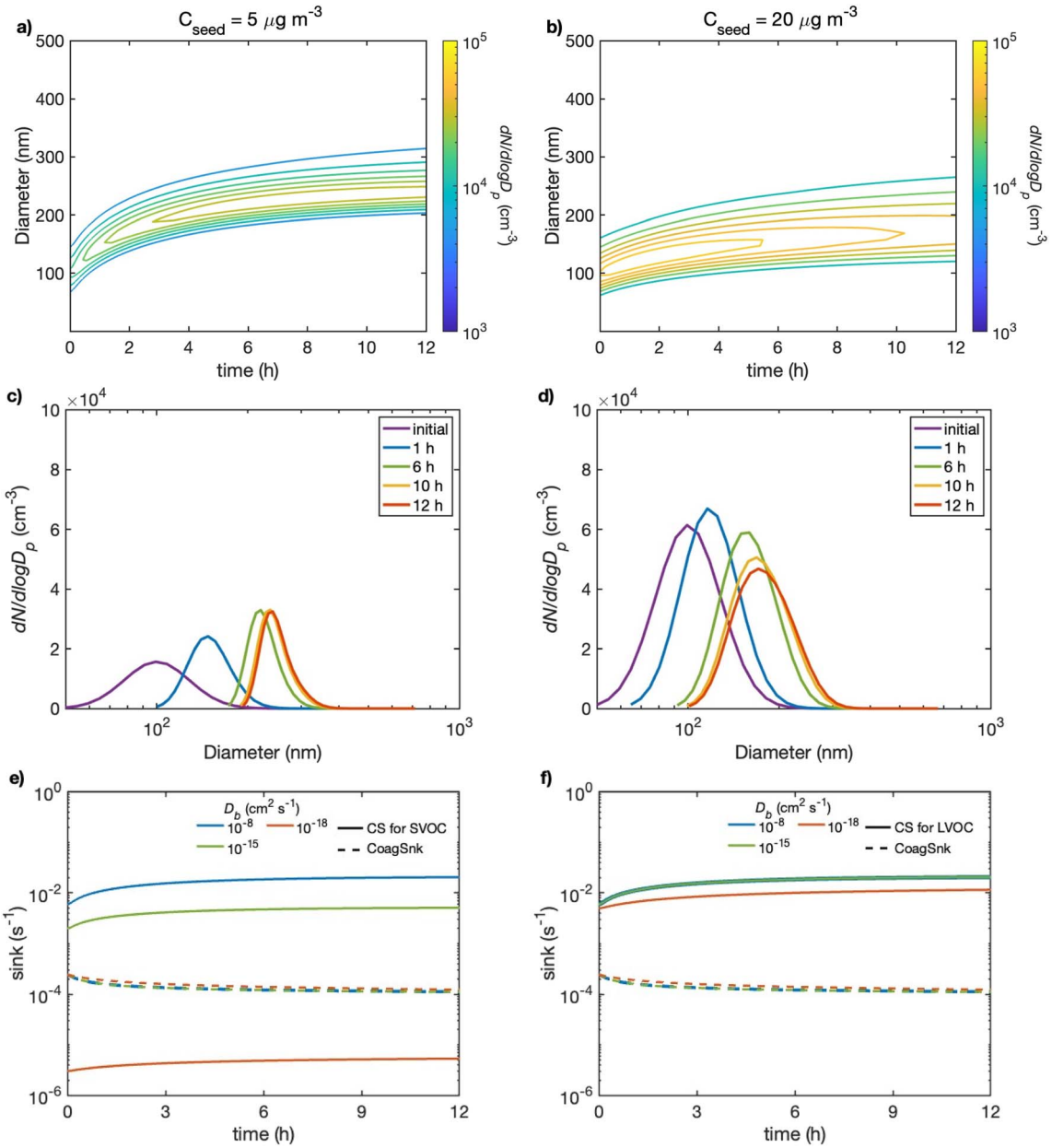

Fig. 3 Modeled evolution of particle number-size distribution in (a and b) contour plots and (c and d) dN/d log D_p at different times for SOA growth in chamber experiments for semi-solid particles ($D_b = 10^{-15}$ cm^2 s^{-1}) with initial seed mass concentrations of (a and c) 5 μg m^{-3} ($N_p = 4 \times 10^3$ cm^{-3}) and (b and d) 20 μg m^{-3} ($N_p = 2 \times 10^4$ cm^{-3}). Coagulation sink (CoagSnk, dashed lines) and condensation sink (CS, solid lines) for (e) SVOC and (f) LVOC calculated for the initial seed concentrations of 5 μg m^{-3} and bulk diffusivities of 10^{-8}, 10^{-15} and 10^{-18} cm^2 s^{-1}.

N_p, exhibiting minor contributions from coagulation. The comparison of the results of Fig. 2 and Fig. S2 emphasizes the importance of the particle size and number concentration. The coagulation coefficient is smaller for large seed particle size, leading to longer coagulation timescales (*e.g.*, Fig. 1).

The effect of the phase state is further investigated by simulating SOA growth with different bulk diffusivities (10^{-8} (liquid), 10^{-15} (semi-solid) and 10^{-18} (ultra-viscous) cm^2 s^{-1}) and calculating coagulation sink (CoagSnk) and condensation sink (CS) for SVOC (Fig. 3e) and LVOC (Fig. 3f). Coagulation sink is initially ~2×10^{-4} s^{-1} and decreases slightly to ~10^{-4} s^{-1} over 12 hours. It is mostly independent of bulk diffusivity, as coagulation is not affected by particle phase state (coagulation efficiency of 1 is assumed for all cases). In contrast, the condensation sink for SVOC depends strongly on bulk diffusivity, being the highest at ~10^{-2} s^{-1} for the liquid, ~2×10^{-3} s^{-1} for the semisolid, and ~3×10^{-6} s^{-1} for the ultra-viscous phase state. This is because the effective mass accommodation coefficient (α_{eff}) is reduced due to kinetic limitations in viscous phase states. For LVOCs, the condensation sink is ~10^{-2} s^{-1} for all phase states, as α_{eff} remains close to unity due to LVOCs' ability to condense effectively irrespective of the

phase state.[52] For liquid and semi-solid states, the condensation sinks of SVOC and LVOC are both higher than the coagulation sinks, confirming that condensation dominates over coagulation. For the ultra-viscous state, the coagulation sink is larger than the condensation sink of SVOC but lower than that of LVOC, indicating that condensation of SVOC is suppressed but condensation of LVOC is still the dominant process. These simulations suggest low aerosol number concentrations, and it is reasonable to assume coagulation has a negligible impact on the overall size distribution. However, under conditions of high particle concentrations, coagulation should be considered for accurate evaluation of particle size distribution as coagulation loss becomes significant (Fig. S3).

Growth of freshly nucleated particles

Freshly nucleated particles can grow *via* condensation, but they can be lost *via* coagulation.[51,64] To investigate this competition in nanoparticle growth, we simulate the growth of freshly nucleated particles in the closed system. We referred to the Cosmics Leaving OUtdoor Droplets (CLOUD) experiments[65] to inform the operating conditions of the experiments. An initial size distribution with a mean diameter of 2 nm was assumed with particle number concentration of 10^5 cm^{-3}.[66] For simplicity, the simulation considers one condensing species, highly oxygenated organic molecules (HOMs) with low volatility ($C^0 = 10^{-4}$ μg m^{-3}) at 263 K, which has been shown to facilitate the initial growth of freshly nucleated particles.[6,67,68] The mass concentrations of HOMs are set at 0.3 μg m^{-3}.[66] The effect of the phase state is considered with different bulk diffusivities ($D_b = 10^{-8}$, 10^{-15} and 10^{-18} cm^2 s^{-1}).

Fig. 4a and b shows the evolution of particle number size distribution for a liquid particle ($D_b = 10^{-8}$ cm^2 s^{-1}). In the first ten minutes, particles grow quickly to 10 nm due to rapid condensation of HOMs with the modeled number-size distribution exhibiting the narrowing characteristic of gas-phase diffusion-limited growth. The particle diameter reaches ~13 nm after 20 min. As the concentration of HOMs decreases further, the peak of the size distribution begins to decrease and stays constant afterwards. There is a local minimum around 14 nm where particles are scavenged efficiently by larger particles, while condensational growth is not yet sufficient to grow

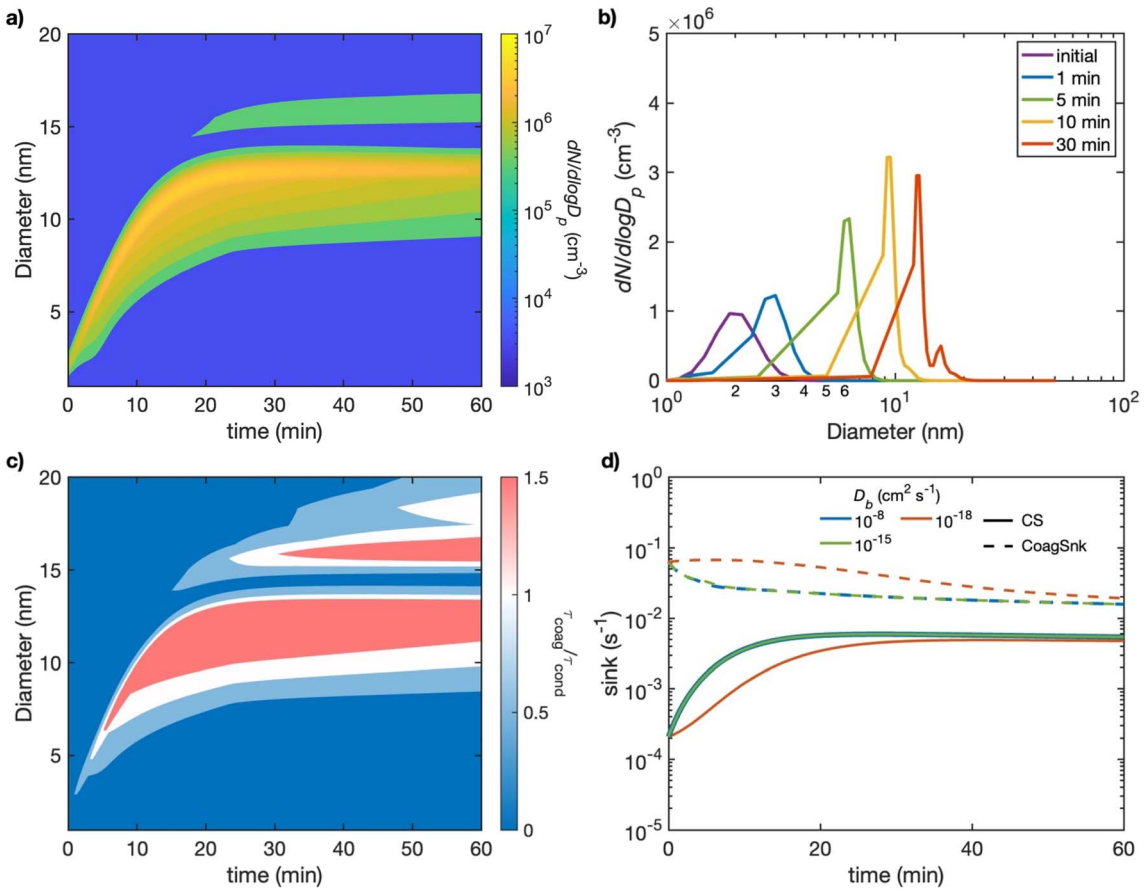

Fig. 4 Modeled evolution of particle number size distribution in (a) contour plot, (b) dN/d log D_p at different times for the growth of freshly nucleated particles with liquid particles ($D_b = 10^{-8}$ cm^2 s^{-1}). (c) Ratio of coagulation timescale to condensation timescale $\left(\frac{\tau_{coag}}{\tau_{cond}}\right)$. Blue color means $\tau_{coag} < \tau_{cond}$, indicating coagulation is favored; red color means $\tau_{coag} > \tau_{cond}$, indicating condensation is favored. (d) Condensation sink (CS, solid lines) and coagulation sink (CoagSnk, dashed lines) calculated with $N_p = 10^5$ cm^{-3} and bulk diffusivities ranging from 10^{-8} to 10^{-18} cm^2 s^{-1}.

this size. After 30 min, a second peak emerges at 16 nm. This bimodal size distribution is indeed observed in continuous flow chamber and CLOUD experiments.[66,69,70] The formation of a bimodal size distribution requires the interplay between condensation and coagulation, as condensation alone cannot form the observed bimodal distribution (see Fig. S4 for simulation without coagulation).

This is further demonstrated in Fig. 4c, showing the ratio of coagulation timescale to condensation timescale $\left(\frac{\tau_{coag}}{\tau_{cond}}\right)$ for liquid particles ($D_b = 10^{-8}$ cm^2 s^{-1}). Initially, τ_{cond} is longer than τ_{coag} for ultrafine particles ($D_p < 5$ nm) as shown in blue color (Fig. 4c), indicating that coagulation proceeds faster than condensation. The condensation of LVOCs to tiny particles is suppressed due to the Kelvin effect. These particles are highly vulnerable to self-coagulation and coagulation scavenging with larger particles. As a result, many freshly nucleated particles are likely lost before condensation can accelerate their growth, reducing the overall number concentrations of these particles. Once the particles increase in size, the Kelvin effect is reduced, thus facilitating condensation of LVOCs. The appearance of a second mode is caused by coagulation growth of larger particles by scavenging smaller particles. Afterwards, condensation becomes increasingly important, as τ_{cond} becomes shorter than τ_{coag} (red area in Fig. 4c). Note that another possible explanation for the observed bimodal distribution for the CLOUD experiments is the rapid co-condensation of nitric acid and ammonia only after the particles reached $D_p \approx$ 4.6 nm,[70] which was not considered in our model simulations. Rapid growth from nitric acid and ammonia condensation could be fast enough to make the freshly nucleated particles less vulnerable to scavenging, thereby increasing their survival probability.

Fig. 4d shows the condensation sink (CS) and coagulation sink (CoagSnk) for simulations with different bulk diffusivities (10^{-8} (liquid), 10^{-15} (semi-solid) and 10^{-18} (ultra-viscous) cm^2 s^{-1}). For all cases, CoagSnk is larger than CS, indicating that coagulation dominates over condensation. This is especially the case during early times, when CS is more than two orders of magnitude lower than CoagSnk. This gap becomes smaller upon growth of nanoparticles to larger sizes allowing CS to become larger; then, condensation becomes a competitive process with coagulation. It is important to note that CS and CoagSnk are calculated for the total particle size distribution, rather than for specific particle sizes. Condensation and coagulation may not impact all particles with different size equally; particles with certain size ranges may experience more significant growth *via* condensation, while others may be vulnerable to coagulation.

CS and CoagSnk behave almost the same for liquid and semisolid particles. For ultra-viscous particles, CoagSnk stays high, and CS increases more slowly due to strong kinetic limitations. In this case, nanoparticles grow slowly, and the formation of bimodal distribution was not observed in the simulations. These results are not consistent with laboratory observations, implying that freshly formed nucleated particles are more likely to adopt a liquid or less-viscous phase state. This behavior is consistent with previous experimental findings, which demonstrated that freshly nucleated particles in the sub 30 nm size range do not exhibit bounce properties due to differences in chemical composition and phase state compared to larger particles.[48] Cheng *et al.* (2015) have suggested that SOA particles at room temperature are expected to be always liquid at diameters below 20 nm due to the nanosize effect.[71] Recent studies have shown that the glass transition temperature can be suppressed substantially upon a decrease of the particle size.[49,50] These implied very small particles ($D_p < 20$ nm) maintain a low-viscous phase state, facilitating the interplay between condensation and coagulation that results in the formation of bimodal size distribution observed in CLOUD chamber experiments. These results emphasize the importance of considering the particle phase state when modeling nucleation and its subsequent growth.

Growth of biomass burning aerosol

To investigate the effect of the phase state on the growth of biomass burning organic aerosols (BBOA), we simulate the temporal evolution of particle number size distribution in fresh smoke in biomass burning plumes with high particle number concentrations. Polydisperse particles with a mean diameter of 130 nm are modeled with $N_p = 3 \times 10^4$ cm^{-3} to represent fresh smoke biomass-burning observations.[72–75] BBOA contains semi-volatile organic compounds (SVOCs), which may evaporate and cause a reduction in particle mass.[76–78] We consider particle population containing SVOC with $C^0 = 1$ μg m^{-3}. The model assumes an open system in which the SVOC concentration in the gas phase is fixed at 0.1, 1, or 10 μg m^{-3} at 298 K to represent a range of concentrations of condensing species, respectively. BBOA can have a wide range of viscosity over a range of relative humidity, so we simulate with different bulk diffusivities ($D_b = 10^{-8}$, 10^{-15}, 10^{-18} cm^2 s^{-1}).[79,80] These simulations allow the evaluation of the influence of the particle phase state on growth dynamics of BBOA. Note that we do not attempt to simulate any specific previously observed biomass burning plumes; instead, we simulate exemplary plume cases that undergo competition among condensation, evaporation and coagulation.

Fig. 5 shows the modeled number size distribution for (a) liquid ($D_b = 10^{-8}$ cm^2 s^{-1}) and (b) ultra-viscous particles ($D_b = 10^{-18}$ cm^2 s^{-1}). For liquid particles, the particle mean diameter decreases from 130 nm to ~100 nm within the first hour driven by the evaporation of SVOC and then increases to ~140 nm over 12 hours. Similar behavior is observed for semi-solid particles (Fig. S5). Fig. 5c shows the particle growth associated with a reduction of the particle number concentration, indicating the major contribution of coagulation. Fig. 5d depicts coagulation (CoagSnk) and condensation sinks (CS), showing that CS is larger than CoagSnk for liquid particles. This indicates that condensation still plays an important role in particle growth, which is especially the case with a higher gas-phase SVOC concentration ($C_g = 1$ μg m^{-3}) (Fig. S6). For ultra-viscous particles, the particle mean diameter increases from 130 nm to ~170 nm over 12 hours. Evaporation and condensation of

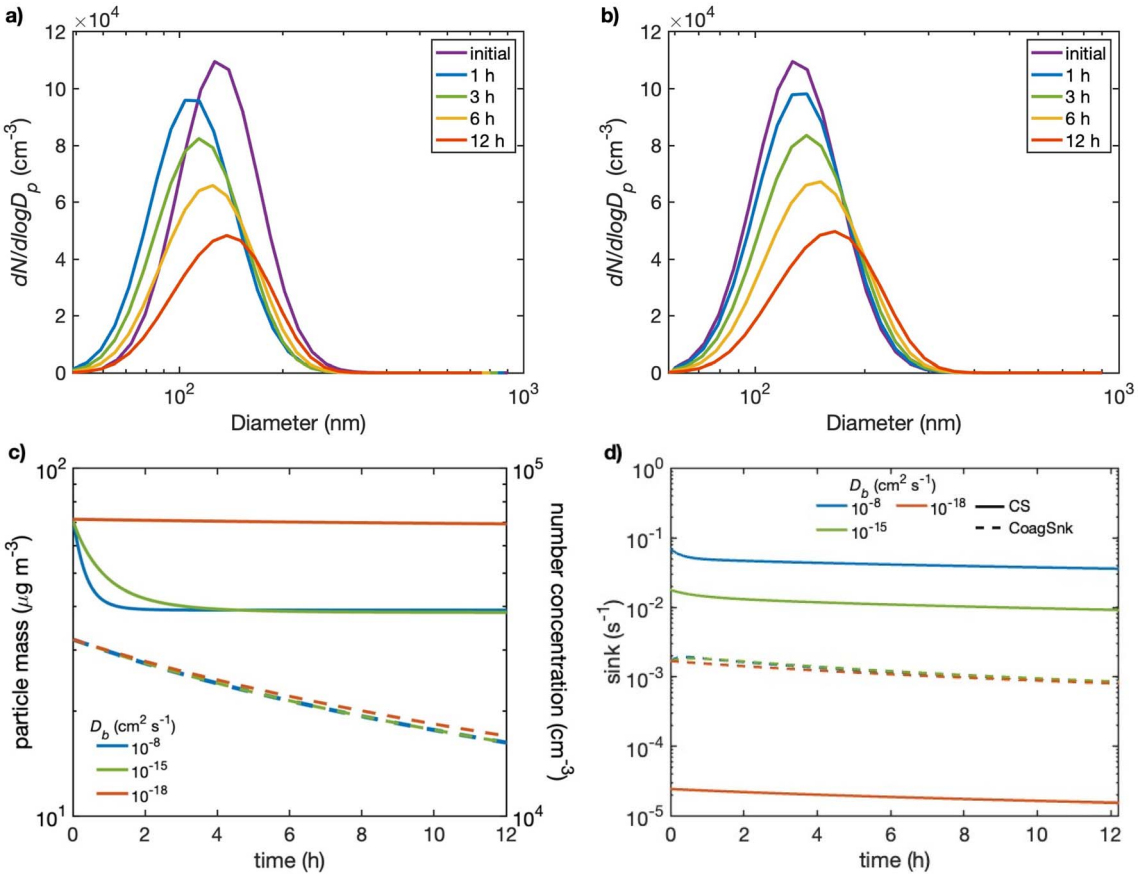

Fig. 5 Modeled number size distribution for the growth of biomass burning organic aerosols with (a) liquid particles ($D_b = 10^{-8}$ cm^2 s^{-1}) and (b) ultra-viscous particles ($D_b = 10^{-18}$ cm^2 s^{-1}) with an SVOC concentration of 0.1 μg m^{-3}. (c) Temporal evolution of particle mass concentration (solid lines, left axis) and particle number concentration (dashed lines, right axis). (d) Condensation sink (CS, solid lines) and coagulation sink (CoagSnk, dashed lines) calculated with bulk diffusivities of 10^{-8}, 10^{-15}, and 10^{-18} cm^2 s^{-1}.

SVOC are both strongly suppressed in viscous particles due to bulk diffusion limitations. CS becomes much smaller than CoagSnk, resulting in primary growth from coagulation. Even with a high gas phase SVOC concentration of 10 μg m^{-3} (Fig. S7) or higher particle number concentration of 4×10^5 cm^{-3} (Fig. S8), the particle growth is driven primarily by coagulation. These simulations are consistent with previous studies,[72,73,75,81] showing that coagulation is the dominant growth mechanism with evaporation and condensation having a relatively minor impact in the smoke plume for highly viscous particles.

These simulations provide useful insights into the competing processes in particle growth under different conditions. Biomass burning plumes are highly variable in term of the composition, particle properties, and atmospheric conditions which can significantly influence the relative importance of condensation, evaporation, and coagulation in particle growth. So, the conclusions drawn from these simulations are specific to the conditions modeled and may not fully capture the complexity of real-world biomass burning plumes.

Discussion and outlook

We have made a few assumptions that may represent the limitations of this study. When two particles coagulate, the resulting particle's composition is assumed to match the composition of the larger particle, even though the composition of the two particles may be different. This may lead to an overestimation or underestimation of semi-volatile species in coagulated particles, potentially affecting τ_{eq} especially for highly viscous particles when coagulation is significant. Another assumption is instantaneous coagulation, even though coalescence of some particles can take a longer time.[82–84] Molecular dynamics simulations have shown that the deformation of the smaller particle dominates the coalescence process in liquid particles, while diffusion processes dominate the coalescence process for solid particles,[85] leading to the longer timescales for the coalescence process. In addition, theoretical calculations and experimental studies showed that viscous effects can retard coagulation rate by an order of magnitude.[86,87] Indeed, Power *et al.* (2013) observed the coalescence timescale of two aerosol particles that combine to form a spherical particle from 10^{-7} to 10^5 s, depending on viscosity.[88] Bell *et al.* (2017) also observed that a solid semi-volatile coating can inhibit the coalescence of coagulating particles for over two days.[89] These studies suggest prolonged coalescence can delay coagulation timescale in highly viscous particles. Further model development is required to incorporate the coalescence process to provide more accurate

representations of the particle size evolution of highly viscous particles.

Nevertheless, our study demonstrates that the competition of condensation and coagulation is affected by the particle phase state. While the coagulation timescale may not be heavily influenced by the phase state, semisolid and ultra-viscous phase states can prolong the equilibration timescales of semi-volatile species substantially. Our results show that condensation plays a dominant role in particle growth at low particle number concentrations for liquid and semi-solid particles, while coagulation can have a significant impact on the evolution of particle size distribution of highly viscous particles at high particle number concentrations. The interplay between condensation and coagulation becomes particularly critical in the growth of freshly nucleated particles, which can lead to the emergence of bimodal size distribution as observed in chamber experiments. This underlines the significant role of coagulation growth in the evolution of particle number size distributions during nanoparticle growth. Additionally, coagulation is the primary cause of growth of highly viscous biomass burning aerosols, where significant particle concentrations can favor coagulation over condensation.

Chamber, flow tube, and modeling studies often simplify the role of coagulation and neglect the competing timescales of condensation and coagulation. We show that this assumption is justified in the cases where the particle phase adopts a low-viscous state with low particle concentrations. If the particle is highly viscous or solid, the diffusion of condensing species significantly hinders mass transport to the bulk, constraining condensation growth and shifting the growth dynamics to favor coagulation. In such cases, ignoring coagulation may lead to inaccurate prediction of the evolution of particle size distributions especially for new particle formation and biomass burning plumes. Proper consideration of the particle phase state is critical for accurate representation of particle size distributions.

Conflicts of interest

We declare no conflict of interests.

Data availability

The simulation data may be obtained from the corresponding author upon request.

Supplementary information is available. See DOI: https://doi.org/10.1039/d5ea00069f.

Acknowledgements

We acknowledge funding from the U. S. National Science Foundation (AGS-2246502 and CHE-2004066) and U.S. Department of Energy (DE-SC0022139 and DE-SC0023042).

References

1 J. L. Jimenez, M. R. Canagaratna, N. M. Donahue, A. S. H. Prevot, Q. Zhang, J. H. Kroll, P. F. Decarlo, J. D. Allan, H. Coe, N. L. Ng, A. C. Aiken, K. S. Docherty, I. M. Ulbrich, A. P. Grieshop, A. L. Robinson, J. Duplissy, J. D. Smith, K. R. Wilson, V. A. Lanz, C. Hueglin, Y. L. Sun, J. Tian, A. Laaksonen, T. Raatikainen, J. Rautiainen, P. Vaattovaara, M. Ehn, M. Kulmala, J. M. Tomlinson, D. R. Collins, M. J. Cubison, J. Dunlea, J. A. Huffman, T. B. Onasch, M. R. Alfarra, P. I. Williams, K. Bower, Y. Kondo, J. Schneider, F. Drewnick, S. Borrmann, S. Weimer, K. Demerjian, D. Salcedo, L. Cottrell, R. Griffin, A. Takami, T. Miyoshi, S. Hatakeyama, A. Shimono, J. Y. Sun, Y. M. Zhang, K. Dzepina, J. R. Kimmel, D. Sueper, J. T. Jayne, S. C. Herndon, A. M. Trimborn, L. R. Williams, E. C. Wood, A. M. Middlebrook, C. E. Kolb, U. Baltensperger and D. R. Worsnop, Evolution of Organic Aerosols in the Atmosphere, *Science*, 2009, **326**, 1525–1529.

2 U. Pöschl and M. Shiraiwa, Multiphase Chemistry at the Atmosphere–Biosphere Interface Influencing Climate and Public Health in the Anthropocene, *Chem. Rev.*, 2015, **115**, 4440–4475.

3 M. Shrivastava, C. D. Cappa, J. Fan, A. H. Goldstein, A. B. Guenther, J. L. Jimenez, C. Kuang, A. Laskin, S. T. Martin, N. L. Ng, T. Petaja, J. R. Pierce, P. J. Rasch, P. Roldin, J. H. Seinfeld, J. Shilling, J. N. Smith, J. A. Thornton, R. Volkamer, J. Wang, D. R. Worsnop, R. A. Zaveri, A. Zelenyuk and Q. Zhang, Recent advances in understanding secondary organic aerosol: Implications for global climate forcing, *Rev. Geophys.*, 2017, **55**, 509–559.

4 M. Kanakidou, J. H. Seinfeld, S. N. Pandis, I. Barnes, F. J. Dentener, M. C. Facchini, R. Van Dingenen, B. Ervens, A. Nenes, C. J. Nielsen, E. Swietlicki, J. P. Putaud, Y. Balkanski, S. Fuzzi, J. Horth, G. K. Moortgat, R. Winterhalter, C. E. L. Myhre, K. Tsigaridis, E. Vignati, E. G. Stephanou and J. Wilson, Organic aerosol and global climate modelling: a review, *Atmos. Chem. Phys.*, 2005, **5**, 1053–1123.

5 P. J. Ziemann and R. Atkinson, Kinetics, products, and mechanisms of secondary organic aerosol formation, *Chem. Soc. Rev.*, 2012, **41**, 6582.

6 J. Tröstl, W. K. Chuang, H. Gordon, M. Heinritzi, C. Yan, U. Molteni, L. Ahlm, C. Frege, F. Bianchi, R. Wagner, M. Simon, K. Lehtipalo, C. Williamson, J. S. Craven, J. Duplissy, A. Adamov, J. Almeida, A.-K. Bernhammer, M. Breitenlechner, S. Brilke, A. Dias, S. Ehrhart, R. C. Flagan, A. Franchin, C. Fuchs, R. Guida, M. Gysel, A. Hansel, C. R. Hoyle, T. Jokinen, H. Junninen, J. Kangasluoma, H. Keskinen, J. Kim, M. Krapf, A. Kürten, A. Laaksonen, M. Lawler, M. Leiminger, S. Mathot, O. Möhler, T. Nieminen, A. Onnela, T. Petäjä, F. M. Piel, P. Miettinen, M. P. Rissanen, L. Rondo, N. Sarnela, S. Schobesberger, K. Sengupta, M. Sipilä, J. N. Smith, G. Steiner, A. Tomè, A. Virtanen, A. C. Wagner, E. Weingartner, D. Wimmer, P. M. Winkler, P. Ye, K. S. Carslaw, J. Curtius, J. Dommen, J. Kirkby, M. Kulmala, I. Riipinen, D. R. Worsnop, N. M. Donahue and U. Baltensperger, The role of low-volatility organic compounds in initial particle growth in the atmosphere, *Nature*, 2016, **533**, 527–531.

7 O. Boucher, D. Randall, P. Artaxo, C. Bretherton, G. Feingold and P. Forster, *Climate Change 2013 – The Physical Science Basis*, 2014, DOI: 10.1017/cbo9781107415324.
8 U. Dusek, G. P. Frank, L. Hildebrandt, J. Curtius, J. Schneider, S. Walter, D. Chand, F. Drewnick, S. Hings, D. Jung, S. Borrmann and M. O. Andreae, Size matters more than chemistry for cloud-nucleating ability of aerosol particles, *Science*, 2006, **312**, 1375–1378.
9 H. Vehkamäki and I. Riipinen, Thermodynamics and kinetics of atmospheric aerosol particle formation and growth, *Chem. Soc. Rev.*, 2012, **41**, 5160–5173.
10 M. Shiraiwa, T. Berkemeier, K. A. Schilling-Fahnestock, J. H. Seinfeld and U. Pöschl, Molecular corridors and kinetic regimes in the multiphase chemical evolution of secondary organic aerosol, *Atmos. Chem. Phys.*, 2014, **14**, 8323–8341.
11 J. F. Pankow, An absorption model of gas/particle partitioning of organic compounds in the atmosphere, *Atmos. Environ.*, 1994, **28**, 185–188.
12 A. Virtanen, J. Joutsensaari, T. Koop, J. Kannosto, P. Yli-Pirilä, J. Leskinen, J. M. Mäkelä, J. K. Holopainen, U. Pöschl, M. Kulmala, D. R. Worsnop and A. Laaksonen, An amorphous solid state of biogenic secondary organic aerosol particles, *Nature*, 2010, **467**, 824–827.
13 T. Koop, J. Bookhold, M. Shiraiwa and U. Pöschl, Glass transition and phase state of organic compounds: dependency on molecular properties and implications for secondary organic aerosols in the atmosphere, *Phys. Chem. Chem. Phys.*, 2011, **13**, 19238.
14 J. P. Reid, A. K. Bertram, D. O. Topping, A. Laskin, S. T. Martin, M. D. Petters, F. D. Pope and G. Rovelli, The viscosity of atmospherically relevant organic particles, *Nat. Commun.*, 2018, **9**, 956.
15 M. Shiraiwa, Y. Li, A. P. Tsimpidi, V. A. Karydis, T. Berkemeier, S. N. Pandis, J. Lelieveld, T. Koop and U. Pöschl, Global distribution of particle phase state in atmospheric secondary organic aerosols, *Nat. Commun.*, 2017, **8**, 15002.
16 R. Luu, M. Schervish, N. A. June, S. E. O'Donnell, S. H. Jathar, J. R. Pierce and M. Shiraiwa, Global Simulations of Phase State and Equilibration Time Scales of Secondary Organic Aerosols with GEOS-Chem, *ACS Earth Space Chem.*, 2025, **9**(2), 288–302.
17 Y. Li, A. G. Carlton and M. Shiraiwa, Diurnal and Seasonal Variations in the Phase State of Secondary Organic Aerosol Material over the Contiguous US Simulated in CMAQ, *ACS Earth Space Chem.*, 2021, **5**, 1971–1982.
18 R. Schmedding, Q. Z. Rasool, Y. Zhang, H. O. T. Pye, H. Zhang, Y. Chen, J. D. Surratt, F. D. Lopez-Hilfiker, J. A. Thornton, A. H. Goldstein and W. Vizuete, Predicting secondary organic aerosol phase state and viscosity and its effect on multiphase chemistry in a regional-scale air quality model, *Atmos. Chem. Phys.*, 2020, **20**, 8201–8225.
19 Z. Zhang, Y. Li, H. Ran, J. An, Y. Qu, W. Zhou, W. Xu, W. Hu, H. Xie, Z. Wang, Y. Sun and M. Shiraiwa, Simulated phase state and viscosity of secondary organic aerosols over China, *Atmos. Chem. Phys.*, 2024, **24**, 4809–4826.
20 Q. Z. Rasool, M. Shrivastava, M. Octaviani, B. Zhao, B. Gaudet and Y. Liu, Modeling Volatility-Based Aerosol Phase State Predictions in the Amazon Rainforest, *ACS Earth Space Chem.*, 2021, **5**, 2910–2924.
21 M. Shiraiwa, M. Ammann, T. Koop and U. Pöschl, Gas uptake and chemical aging of semisolid organic aerosol particles, *Proc. Natl. Acad. Sci. U. S. A.*, 2011, **108**, 11003–11008.
22 A. M. Maclean, C. L. Butenhoff, J. W. Grayson, K. Barsanti, J. L. Jimenez and A. K. Bertram, Mixing times of organic molecules within secondary organic aerosol particles: a global planetary boundary layer perspective, *Atmos. Chem. Phys.*, 2017, **17**, 13037–13048.
23 Q. Mu, M. Shiraiwa, M. Octaviani, N. Ma, A. Ding, H. Su, G. Lammel, U. Pöschl and Y. Cheng, Temperature effect on phase state and reactivity controls atmospheric multiphase chemistry and transport of PAHs, *Sci. Adv.*, 2018, **4**, eaap7314.
24 M. Shrivastava, S. Lou, A. Zelenyuk, R. C. Easter, R. A. Corley, B. D. Thrall, P. J. Rasch, J. D. Fast, S. L. Massey Simonich, H. Shen and S. Tao, Global long-range transport and lung cancer risk from polycyclic aromatic hydrocarbons shielded by coatings of organic aerosol, *Proc. Natl. Acad. Sci. U. S. A.*, 2017, **114**, 1246–1251.
25 M. Schervish and M. Shiraiwa, Impact of phase state and non-ideal mixing on equilibration timescales of secondary organic aerosol partitioning, *Atmos. Chem. Phys.*, 2023, **23**, 221–233.
26 M. Schervish, N. M. Donahue and M. Shiraiwa, Effects of volatility, viscosity, and non-ideality on particle–particle mixing timescales of secondary organic aerosols, *Aerosol Sci. Technol.*, 2024, **58**, 411–426.
27 Q. Ye, M. A. Upshur, E. S. Robinson, F. M. Geiger, R. C. Sullivan, R. J. Thomson and N. M. Donahue, Following Particle-Particle Mixing in Atmospheric Secondary Organic Aerosols by Using Isotopically Labeled Terpenes, *Chem*, 2018, **4**, 318–333.
28 M. Shiraiwa, L. D. Yee, K. A. Schilling, C. L. Loza, J. S. Craven, A. Zuend, P. J. Ziemann and J. H. Seinfeld, Size distribution dynamics reveal particle-phase chemistry in organic aerosol formation, *Proc. Natl. Acad. Sci. U. S. A.*, 2013, **110**, 11746–11750.
29 R. A. Zaveri, J. E. Shilling, A. Zelenyuk, J. Liu, D. M. Bell, E. L. D'Ambro, C. J. Gaston, J. A. Thornton, A. Laskin, P. Lin, J. Wilson, R. C. Easter, J. Wang, A. K. Bertram, S. T. Martin, J. H. Seinfeld and D. R. Worsnop, Growth Kinetics and Size Distribution Dynamics of Viscous Secondary Organic Aerosol, *Environ. Sci. Technol.*, 2018, **52**, 1191–1199.
30 R. A. Zaveri, J. E. Shilling, A. Zelenyuk, M. A. Zawadowicz, K. Suski, S. China, D. M. Bell, D. Veghte and A. Laskin, Particle-Phase Diffusion Modulates Partitioning of Semivolatile Organic Compounds to Aged Secondary Organic Aerosol, *Environ. Sci. Technol.*, 2020, **54**, 2595–2605.
31 R. A. Zaveri, J. Wang, J. Fan, Y. Zhang, J. E. Shilling, A. Zelenyuk, F. Mei, R. Newsom, M. Pekour, J. Tomlinson, J. M. Comstock, M. Shrivastava, E. Fortner,

L. A. T. Machado, P. Artaxo and S. T. Martin, Rapid growth of anthropogenic organic nanoparticles greatly alters cloud life cycle in the Amazon rainforest, *Sci. Adv.*, 2022, **8**(2), eabj0329.

32 Y. He, A. Akherati, T. Nah, N. L. Ng, L. A. Garofalo, D. K. Farmer, M. Shiraiwa, R. A. Zaveri, C. D. Cappa, J. R. Pierce and S. H. Jathar, Particle Size Distribution Dynamics Can Help Constrain the Phase State of Secondary Organic Aerosol, *Environ. Sci. Technol.*, 2021, **55**, 1466–1476.

33 M. Shrivastava, Q. Z. Rasool, B. Zhao, M. Octaviani, R. A. Zaveri, A. Zelenyuk, B. Gaudet, Y. Liu, J. E. Shilling, J. Schneider, C. Schulz, M. Zöger, S. T. Martin, J. Ye, A. Guenther, R. F. Souza, M. Wendisch and U. Pöschl, Tight Coupling of Surface and In-Plant Biochemistry and Convection Governs Key Fine Particulate Components over the Amazon Rainforest, *ACS Earth Space Chem.*, 2022, **6**, 380–390.

34 R. A. Zaveri, R. C. Easter, J. E. Shilling and J. H. Seinfeld, Modeling kinetic partitioning of secondary organic aerosol and size distribution dynamics: representing effects of volatility, phase state, and particle-phase reaction, *Atmos. Chem. Phys.*, 2014, **14**, 5153–5181.

35 C. Le, N. Xu, Q. Li, D. R. Collins and D. R. Cocker, Experimental characterization of particle wall-loss behaviors in UCR dual-90m ^{3} Teflon chambers, *Aerosol Sci. Technol.*, 2024, **58**, 288–300.

36 M. S. Taylor Jr, D. N. Higgins, J. M. Krasnomowitz and M. V. Johnston, Ultrafine Particle Growth Rate During Biogenic Secondary Organic Matter Formation as a Function of Particle Composition, Size, and Phase, *ACS ES&T Air*, 2025, **2**, 615–624.

37 M. Shiraiwa, C. Pfrang, T. Koop and U. Pöschl, Kinetic multi-layer model of gas-particle interactions in aerosols and clouds (KM-GAP): linking condensation, evaporation and chemical reactions of organics, oxidants and water, *Atmos. Chem. Phys.*, 2012, **12**, 2777–2794.

38 J. H. Seinfeld and S. N. Pandis, *Atmospheric Chemistry and Physics : from Air Pollution to Climate Change*, John Wiley & Sons, Inc., Hoboken, New Jersey, 3rd edn, 2016.

39 M. Z. Jacobson and R. P. Turco, Simulating Condensational Growth, Evaporation, and Coagulation of Aerosols Using a Combined Moving and Stationary Size Grid, *Aerosol Sci. Technol.*, 1995, **22**, 73–92.

40 M. Z. Jacobson, D. B. Kittelson and W. F. Watts, Enhanced Coagulation Due to Evaporation and Its Effect on Nanoparticle Evolution, *Environ. Sci. Technol.*, 2005, **39**, 9486–9492.

41 J. Julin, P. M. Winkler, N. M. Donahue, P. E. Wagner and I. Riipinen, Near-Unity Mass Accommodation Coefficient of Organic Molecules of Varying Structure, *Environ. Sci. Technol.*, 2014, **48**, 12083–12089.

42 M. Von Domaros, P. S. J. Lakey, M. Shiraiwa and D. J. Tobias, Multiscale Modeling of Human Skin Oil-Induced Indoor Air Chemistry: Combining Kinetic Models and Molecular Dynamics, *J. Phys. Chem. B*, 2020, **124**, 3836–3843.

43 Y. Li and M. Shiraiwa, Timescales of secondary organic aerosols to reach equilibrium at various temperatures and relative humidities, *Atmos. Chem. Phys.*, 2019, **19**, 5959–5971.

44 V.-M. Kerminen, K. E. J. Lehtinen, T. Anttila and M. Kulmala, Dynamics of atmospheric nucleation mode particles: a timescale analysis, *Tellus B*, 2004, **56**, 135–146.

45 A. D'Alessio, A. C. Barone, R. Cau, A. D'Anna and P. Minutolo, Surface deposition and coagulation efficiency of combustion generated nanoparticles in the size range from 1 to 10 nm, *Proc. Combust. Inst.*, 2005, **30**, 2595–2603.

46 G. Narsimhan and E. Ruckenstein, Monte Carlo simulation of brownian coagulation over the entire range of particle sizes from near molecular to colloidal: Connection between collision efficiency and interparticle forces, *J. Colloid Interface Sci.*, 1985, **107**, 174–193.

47 D. Hou, D. Zong, C. S. Lindberg, M. Kraft and X. You, On the coagulation efficiency of carbonaceous nanoparticles, *J. Aerosol Sci.*, 2020, **140**, 105478.

48 A. Virtanen, J. Kannosto, H. Kuuluvainen, A. Arffman, J. Joutsensaari, E. Saukko, L. Hao, P. Yli-Pirilä, P. Tiitta, J. K. Holopainen, J. Keskinen, D. R. Worsnop, J. N. Smith and A. Laaksonen, Bounce behavior of freshly nucleated biogenic secondary organic aerosol particles, *Atmos. Chem. Phys.*, 2011, **11**, 8759–8766.

49 S. Mahant, J. R. Snider, S. S. Petters and M. D. Petters, Effect of Aerosol Size on Glass Transition Temperature, *J. Phys. Chem. Lett.*, 2024, **15**, 7509–7515.

50 M. Petters and S. Kasparoglu, Predicting the influence of particle size on the glass transition temperature and viscosity of secondary organic material, *Sci. Rep.*, 2020, **10**, 15170.

51 M. Kulmala, M. D. Maso, J. M. Makela, L. Pirjola, M. Vakeva, P. Aalto, P. Miikkulainen, K. Hameri and C. D. O'Dowd, On the formation, growth and composition of nucleation mode particles, *Tellus B*, 2001, **53**, 479–490.

52 M. Shiraiwa and U. Pöschl, Mass accommodation and gas–particle partitioning in secondary organic aerosols: dependence on diffusivity, volatility, particle-phase reactions, and penetration depth, *Atmos. Chem. Phys.*, 2021, **21**, 1565–1580.

53 C. Rose, M. Collaud Coen, E. Andrews, Y. Lin, I. Bossert, C. Lund Myhre, T. Tuch, A. Wiedensohler, M. Fiebig, P. Aalto, A. Alastuey, E. Alonso-Blanco, M. Andrade, B. Artíñano, T. Arsov, U. Baltensperger, S. Bastian, O. Bath, J. P. Beukes, B. T. Brem, N. Bukowiecki, J. A. Casquero-Vera, S. Conil, K. Eleftheriadis, O. Favez, H. Flentje, M. I. Gini, F. J. Gómez-Moreno, M. Gysel-Beer, A. G. Hallar, I. Kalapov, N. Kalivitis, A. Kasper-Giebl, M. Keywood, J. E. Kim, S.-W. Kim, A. Kristensson, M. Kulmala, H. Lihavainen, N.-H. Lin, H. Lyamani, A. Marinoni, S. Martins Dos Santos, O. L. Mayol-Bracero, F. Meinhardt, M. Merkel, J.-M. Metzger, N. Mihalopoulos, J. Ondracek, M. Pandolfi, N. Pérez, T. Petäjä, J.-E. Petit, D. Picard, J.-M. Pichon, V. Pont, J.-P. Putaud, F. Reisen, K. Sellegri, S. Sharma, G. Schauer, P. Sheridan, J. P. Sherman, A. Schwerin, R. Sohmer, M. Sorribas, J. Sun, P. Tulet, V. Vakkari, P. G. Van Zyl, F. Velarde, P. Villani, S. Vratolis,

Z. Wagner, S.-H. Wang, K. Weinhold, R. Weller, M. Yela, V. Zdimal and P. Laj, Seasonality of the particle number concentration and size distribution: a global analysis retrieved from the network of Global Atmosphere Watch (GAW) near-surface observatories, *Atmos. Chem. Phys.*, 2021, **21**, 17185–17223.

54 S. Gani, S. Bhandari, K. Patel, S. Seraj, P. Soni, Z. Arub, G. Habib, L. Hildebrandt Ruiz and J. S. Apte, Particle number concentrations and size distribution in a polluted megacity: the Delhi Aerosol Supersite study, *Atmos. Chem. Phys.*, 2020, **20**, 8533–8549.

55 M. Shiraiwa and J. H. Seinfeld, Equilibration timescale of atmospheric secondary organic aerosol partitioning, *Geophys. Res. Lett.*, 2012, **39**(24), L24801.

56 I. Riipinen, J. R. Pierce, T. Yli-Juuti, T. Nieminen, S. Häkkinen, M. Ehn, H. Junninen, K. Lehtipalo, T. Petäjä, J. Slowik, R. Chang, N. C. Shantz, J. Abbatt, W. R. Leaitch, V. M. Kerminen, D. R. Worsnop, S. N. Pandis, N. M. Donahue and M. Kulmala, Organic condensation: a vital link connecting aerosol formation to cloud condensation nuclei (CCN) concentrations, *Atmos. Chem. Phys.*, 2011, **11**, 3865–3878.

57 H. Mai, M. Shiraiwa, R. C. Flagan and J. H. Seinfeld, Under What Conditions Can Equilibrium Gas–Particle Partitioning Be Expected to Hold in the Atmosphere?, *Environ. Sci. Technol.*, 2015, **49**, 11485–11491.

58 R. J. Griffin, D. R. Cocker, R. C. Flagan and J. H. Seinfeld, Organic aerosol formation from the oxidation of biogenic hydrocarbons, *J. Geophys. Res.: Atmos.*, 1999, **104**, 3555–3567.

59 R. K. Pathak, C. O. Stanier, N. M. Donahue and S. N. Pandis, Ozonolysis of α-pinene at atmospherically relevant concentrations: Temperature dependence of aerosol mass fractions (yields), *J. Geophys. Res.: Atmos.*, 2007, **112**, D03201.

60 C.-W. Chu, J. Zhai, Y. Han, J. Ye, R. A. Zaveri, S. T. Martin and H.-M. Hung, New Particle Formation and Growth Dynamics for α-Pinene Ozonolysis in a Smog Chamber and Implications for Ambient Environments, *ACS Earth Space Chem.*, 2022, **6**, 2826–2835.

61 V. G. Khamaganov and R. A. Hites, Rate Constants for the Gas-Phase Reactions of Ozone with Isoprene, α- and β-Pinene, and Limonene as a Function of Temperature, *J. Phys. Chem. A*, 2001, **105**, 815–822.

62 X. Zhang, S. N. Pandis and J. H. Seinfeld, Diffusion-Limited Versus Quasi-Equilibrium Aerosol Growth, *Aerosol Sci. Technol.*, 2012, **46**, 874–885.

63 J. F. Hunter, A. J. Carrasquillo, K. E. Daumit and J. H. Kroll, Secondary Organic Aerosol Formation from Acyclic, Monocyclic, and Polycyclic Alkanes, *Environ. Sci. Technol.*, 2014, **48**, 10227–10234.

64 C. Kuang, I. Riipinen, S. L. Sihto, M. Kulmala, A. V. McCormick and P. H. McMurry, An improved criterion for new particle formation in diverse atmospheric environments, *Atmos. Chem. Phys.*, 2010, **10**, 8469–8480.

65 J. Kirkby, J. Curtius, J. Almeida, E. Dunne, J. Duplissy, S. Ehrhart, A. Franchin, S. Gagné, L. Ickes, A. Kürten, A. Kupc, A. Metzger, F. Riccobono, L. Rondo, S. Schobesberger, G. Tsagkogeorgas, D. Wimmer, A. Amorim, F. Bianchi, M. Breitenlechner, A. David, J. Dommen, A. Downard, M. Ehn, R. C. Flagan, S. Haider, A. Hansel, D. Hauser, W. Jud, H. Junninen, F. Kreissl, A. Kvashin, A. Laaksonen, K. Lehtipalo, J. Lima, E. R. Lovejoy, V. Makhmutov, S. Mathot, J. Mikkilä, P. Minginette, S. Mogo, T. Nieminen, A. Onnela, P. Pereira, T. Petäjä, R. Schnitzhofer, J. H. Seinfeld, M. Sipilä, Y. Stozhkov, F. Stratmann, A. Tomé, J. Vanhanen, Y. Viisanen, A. Vrtala, P. E. Wagner, H. Walther, E. Weingartner, H. Wex, P. M. Winkler, K. S. Carslaw, D. R. Worsnop, U. Baltensperger and M. Kulmala, Role of sulphuric acid, ammonia and galactic cosmic rays in atmospheric aerosol nucleation, *Nature*, 2011, **476**, 429–433.

66 W. Kong, S. Amanatidis, H. Mai, C. Kim, B. C. Schulze, Y. Huang, G. S. Lewis, S. V. Hering, J. H. Seinfeld and R. C. Flagan, The nano-scanning electrical mobility spectrometer (nSEMS) and its application to size distribution measurements of 1.5–25 nm particles, *Atmos. Meas. Tech.*, 2021, **14**, 5429–5445.

67 D. Stolzenburg, L. Fischer, A. L. Vogel, M. Heinritzi, M. Schervish, M. Simon, A. C. Wagner, L. Dada, L. R. Ahonen, A. Amorim, A. Baccarini, P. S. Bauer, B. Baumgartner, A. Bergen, F. Bianchi, M. Breitenlechner, S. Brilke, S. Buenrostro Mazon, D. Chen, A. Dias, D. C. Draper, J. Duplissy, I. El Haddad, H. Finkenzeller, C. Frege, C. Fuchs, O. Garmash, H. Gordon, X. He, J. Helm, V. Hofbauer, C. R. Hoyle, C. Kim, J. Kirkby, J. Kontkanen, A. Kürten, J. Lampilahti, M. Lawler, K. Lehtipalo, M. Leiminger, H. Mai, S. Mathot, B. Mentler, U. Molteni, W. Nie, T. Nieminen, J. B. Nowak, A. Ojdanic, A. Onnela, M. Passananti, T. Petäjä, L. L. J. Quéléver, M. P. Rissanen, N. Sarnela, S. Schallhart, C. Tauber, A. Tomé, R. Wagner, M. Wang, L. Weitz, D. Wimmer, M. Xiao, C. Yan, P. Ye, Q. Zha, U. Baltensperger, J. Curtius, J. Dommen, R. C. Flagan, M. Kulmala, J. N. Smith, D. R. Worsnop, A. Hansel, N. M. Donahue and P. M. Winkler, Rapid growth of organic aerosol nanoparticles over a wide tropospheric temperature range, *Proc. Natl. Acad. Sci. U. S. A.*, 2018, **115**, 9122–9127.

68 F. Bianchi, T. Kurtén, M. Riva, C. Mohr, M. P. Rissanen, P. Roldin, T. Berndt, J. D. Crounse, P. O. Wennberg, T. F. Mentel, J. Wildt, H. Junninen, T. Jokinen, M. Kulmala, D. R. Worsnop, J. A. Thornton, N. Donahue, H. G. Kjaergaard and M. Ehn, Highly Oxygenated Organic Molecules (HOM) from Gas-Phase Autoxidation Involving Peroxy Radicals: A Key Contributor to Atmospheric Aerosol, *Chem. Rev.*, 2019, **119**, 3472–3509.

69 J. Zhao, J. Ortega, M. Chen, P. H. McMurry and J. N. Smith, Dependence of particle nucleation and growth on high-molecular-weight gas-phase products during ozonolysis of α-pinene, *Atmos. Chem. Phys.*, 2013, **13**, 7631–7644.

70 M. Wang, W. Kong, R. Marten, X.-C. He, D. Chen, J. Pfeifer, A. Heitto, J. Kontkanen, L. Dada, A. Kürten, T. Yli-Juuti, H. E. Manninen, S. Amanatidis, A. Amorim, R. Baalbaki, A. Baccarini, D. M. Bell, B. Bertozzi, S. Bräkling, S. Brilke, L. C. Murillo, R. Chiu, B. Chu, L.-P. De Menezes, J. Duplissy, H. Finkenzeller, L. G. Carracedo, M. Granzin,

R. Guida, A. Hansel, V. Hofbauer, J. Krechmer, K. Lehtipalo, H. Lamkaddam, M. Lampimäki, C. P. Lee, V. Makhmutov, G. Marie, S. Mathot, R. L. Mauldin, B. Mentler, T. Müller, A. Onnela, E. Partoll, T. Petäjä, M. Philippov, V. Pospisilova, A. Ranjithkumar, M. Rissanen, B. Rörup, W. Scholz, J. Shen, M. Simon, M. Sipilä, G. Steiner, D. Stolzenburg, Y. J. Tham, A. Tomé, A. C. Wagner, D. S. Wang, Y. Wang, S. K. Weber, P. M. Winkler, P. J. Wlasits, Y. Wu, M. Xiao, Q. Ye, M. Zauner-Wieczorek, X. Zhou, R. Volkamer, I. Riipinen, J. Dommen, J. Curtius, U. Baltensperger, M. Kulmala, D. R. Worsnop, J. Kirkby, J. H. Seinfeld, I. El-Haddad, R. C. Flagan and N. M. Donahue, Rapid growth of new atmospheric particles by nitric acid and ammonia condensation, *Nature*, 2020, **581**, 184–189.

71 Y. Cheng, H. Su, T. Koop, E. Mikhailov and U. Pöschl, Size dependence of phase transitions in aerosol nanoparticles, *Nat. Commun.*, 2015, **6**, 5923.

72 K. M. Sakamoto, J. D. Allan, H. Coe, J. W. Taylor, T. J. Duck and J. R. Pierce, Aged boreal biomass-burning aerosol size distributions from BORTAS 2011, *Atmos. Chem. Phys.*, 2015, **15**, 1633–1646.

73 K. M. Sakamoto, J. R. Laing, R. G. Stevens, D. A. Jaffe and J. R. Pierce, The evolution of biomass-burning aerosol size distributions due to coagulation: dependence on fire and meteorological details and parameterization, *Atmos. Chem. Phys.*, 2016, **16**, 7709–7724.

74 E. J. T. Levin, G. R. McMeeking, C. M. Carrico, L. E. Mack, S. M. Kreidenweis, C. E. Wold, H. Moosmüller, W. P. Arnott, W. M. Hao, J. L. Collett and W. C. Malm, Biomass burning smoke aerosol properties measured during Fire Laboratory at Missoula Experiments (FLAME), *J. Geophys. Res.: Atmos.*, 2010, **115**, D18210.

75 N. A. June, A. L. Hodshire, E. B. Wiggins, E. L. Winstead, C. E. Robinson, K. L. Thornhill, K. J. Sanchez, R. H. Moore, D. Pagonis, H. Guo, P. Campuzano-Jost, J. L. Jimenez, M. M. Coggon, J. M. Dean-Day, T. P. Bui, J. Peischl, R. J. Yokelson, M. J. Alvarado, S. M. Kreidenweis, S. H. Jathar and J. R. Pierce, Aerosol size distribution changes in FIREX-AQ biomass burning plumes: the impact of plume concentration on coagulation and OA condensation/evaporation, *Atmos. Chem. Phys.*, 2022, **22**, 12803–12825.

76 L. A. Garofalo, M. A. Pothier, E. J. T. Levin, T. Campos, S. M. Kreidenweis and D. K. Farmer, Emission and Evolution of Submicron Organic Aerosol in Smoke from Wildfires in the Western United States, *ACS Earth Space Chem.*, 2019, **3**, 1237–1247.

77 A. A. May, E. J. T. Levin, C. J. Hennigan, I. Riipinen, T. Lee, J. L. Collett, J. L. Jimenez, S. M. Kreidenweis and A. L. Robinson, Gas-particle partitioning of primary organic aerosol emissions: 3. Biomass burning, *J. Geophys. Res.: Atmos.*, 2013, **118**(11), 327–311.

78 J. A. Huffman, K. S. Docherty, A. C. Aiken, M. J. Cubison, I. M. Ulbrich, P. F. Decarlo, D. Sueper, J. T. Jayne, D. R. Worsnop, P. J. Ziemann and J. L. Jimenez, Chemically-resolved aerosol volatility measurements from two megacity field studies, *Atmos. Chem. Phys.*, 2009, **9**, 7161–7182.

79 Y. Huang, F. Mahrt, S. Xu, M. Shiraiwa, A. Zuend and A. K. Bertram, Coexistence of three liquid phases in individual atmospheric aerosol particles, *Proc. Natl. Acad. Sci. U. S. A.*, 2021, **118**, e2102512118.

80 N. G. A. Gerrebos, J. Zaks, F. K. A. Gregson, M. Walton-Raaby, H. Meeres, I. Zigg, W. F. Zandberg and A. K. Bertram, High Viscosity and Two Phases Observed over a Range of Relative Humidities in Biomass Burning Organic Aerosol from Canadian Wildfires, *Environ. Sci. Technol.*, 2024, **58**, 21716–21728.

81 A. L. Hodshire, Q. Bian, E. Ramnarine, C. R. Lonsdale, M. J. Alvarado, S. M. Kreidenweis, S. H. Jathar and J. R. Pierce, More Than Emissions and Chemistry: Fire Size, Dilution, and Background Aerosol Also Greatly Influence Near-Field Biomass Burning Aerosol Aging, *J. Geophys. Res.: Atmos.*, 2019, **124**, 5589–5611.

82 P. S. Lee and D. T. Shaw, Dynamics of Fibrous-Type Particles: Brownian Coagulation and the Charge Effect, *Aerosol Sci. Technol.*, 1984, **3**, 9–16.

83 V. I. Gryn and M. K. Kerimov, Integrodifferential equations for non-spherical aerosols coagulation, *USSR Comput. Math. Math. Phys.*, 1990, **30**, 211–224.

84 S. N. Rogak and R. C. Flagan, Coagulation of aerosol agglomerates in the transition regime, *J. Colloid Interface Sci.*, 1992, **151**, 203–224.

85 T. Hawa and M. R. Zachariah, Coalescence kinetics of unequal sized nanoparticles, *J. Aerosol Sci.*, 2006, **37**, 1–15.

86 L. A. Spielman, Viscous interactions in Brownian coagulation, *J. Colloid Interface Sci.*, 1970, **33**, 562–571.

87 K. Higashitani, M. Kondo and S. Hatade, Effect of particle size on coagulation rate of ultrafine colloidal particles, *J. Colloid Interface Sci.*, 1991, **142**, 204–213.

88 R. M. Power, S. H. Simpson, J. P. Reid and A. J. Hudson, The transition from liquid to solid-like behaviour in ultrahigh viscosity aerosol particles, *Chem. Sci.*, 2013, **4**, 2597.

89 D. M. Bell, D. Imre, S. T. Martin and A. Zelenyuk, The properties and behavior of α-pinene secondary organic aerosol particles exposed to ammonia under dry conditions, *Phys. Chem. Chem. Phys.*, 2017, **19**, 6497–6507.

